Optics and Lasers in Engineering 181 (2024) 108448

Contents lists available at ScienceDirect

Optics and Lasers in Engineering

journal homepage: www.elsevier.com/locate/optlaseng

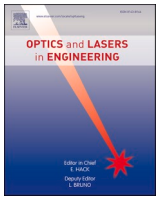

Digital image correlation approach for low-cycle fatigue life monitoring of 13HMF power engineering steel

Mateusz Kopec

Institute of Fundamental Technological Research, Polish Academy of Sciences, 5b Pawińskiego Str. 02-106, Warsaw, Poland

ARTICLE INFO

Keywords:
Fatigue
Mechanical properties
Strain analysis, Digital image correlation

ABSTRACT

In this paper, strain evolution of 13HMF power engineering steel was analysed during force-controlled low cycle fatigue (LCF). The material performance under cyclic loading was monitored by using Digital Image Correlation (DIC) technique for different values of stress amplitude exceeding the yield strength of the material significantly. Data collected from DIC was compared to the extensometer ones to confirm the effectiveness of the proposed approach. Finally, the cloud data reflecting the fatigue performance of 13HMF was generated in the form of strain-stress amplitude - service life distribution map.

1. Introduction

Power engineering steels are specifically designed for pressure components operating at high temperature. In this group, the 13HMF chromium-molybdenum-vanadium steel is commonly used as material for boiler tubes, steam turbine parts, and boilers operating at a temperature up to 560 °C. The deterioration of these components is primarily caused by the extreme service conditions they experience during operation. Such harsh conditions accelerate the damage development dynamics [1]. Therefore, it is crucial to continuously monitor the condition of power engineering steel structures to ensure their safety and avoid the operational costs associated with enforced shutdowns.

Thermal fluctuations experienced during the shutdowns of power plant stations lead to significant alterations in the microstructure of materials, thereby impacting their mechanical properties. The occurrence of high-temperature gradients and internal pressure variations within pipes further contribute to the introduction of external and internal stresses. These stresses have the potential to surpass the material's yield strength, leading to plastic deformation [2]. Therefore, investigating the analysis of low cycle fatigue (LCF) response of power engineering steels in the plastic regime is extremely important to maintain the safe operation of power plant components and to further predict their remaining service life.

Comprehensive health monitoring of power engineering steel structures requires detailed mechanical investigations to effectively evaluate the deterioration of the material after prolonged service. These analyses typically involve standard tensile [3], Charpy [3], creep [4-6], and fatigue [1] tests. However, it is important to note that the conventional S–N curve only provides limited information, namely stress amplitude and a corresponding number of cycles to failure. Furthermore, the strain changes are frequently monitored by using extensometers and tensometers, which offer continuous monitoring of strain changes during testing. However, they provide average data from the measurements performed on a limited gauge section of the specimen. Such an issue is a serious limitation, particularly in crack predictions since both these techniques are unable to accurately predict and localise crack initiation within the gauge length. Consequently, it is necessary to rely on material models and finite element simulations for this purpose. Such crack localisation and development could be, however, effectively predicted and monitored by utilising full-field optical methods [7]. Among these methods, DIC is known for its wide adoption in mechanical testing. DIC involves the application of two CCD cameras, light sources, and computational software. Before testing, the specimen is covered with a pattern consisting of black dots on a bright background [8]. The pattern defines the x and z coordinates, which are essential for conducting tests under strain control. The displacement/strain is calculated by applying rectangular or square-shaped patterns directly onto the specimen surface. The results are then displayed in the form of full-field strain distribution maps [9]. DIC was primarily utilised for static measurements, focusing on tensile and compressive behaviour, fracture toughness, and the impact of geometrical imperfections on mechanical response [10, 11]. The development in experimental testing significantly expanded the application of DIC. Furthermore, DIC offers solutions to various issues that traditional contact sensors like extensometers and strain gauges cannot address. These include extensometer slippage, potential damage to the sensor from specimen fractures, exceeding the

E-mail address: mkopec@ippt.pan.pl.

https://doi.org/10.1016/j.optlaseng.2024.108448
Received 29 May 2024; Received in revised form 11 July 2024; Accepted 18 July 2024

Table 1
Chemical composition of 13HMF steel in as-received condition

Element	C	Si	Mn	P	S	Cr	Mo	Ni	Fe
wt [%]	0.15	0.30	0.60	0.02	0.02	0.55	0.55	0.25	Bal.

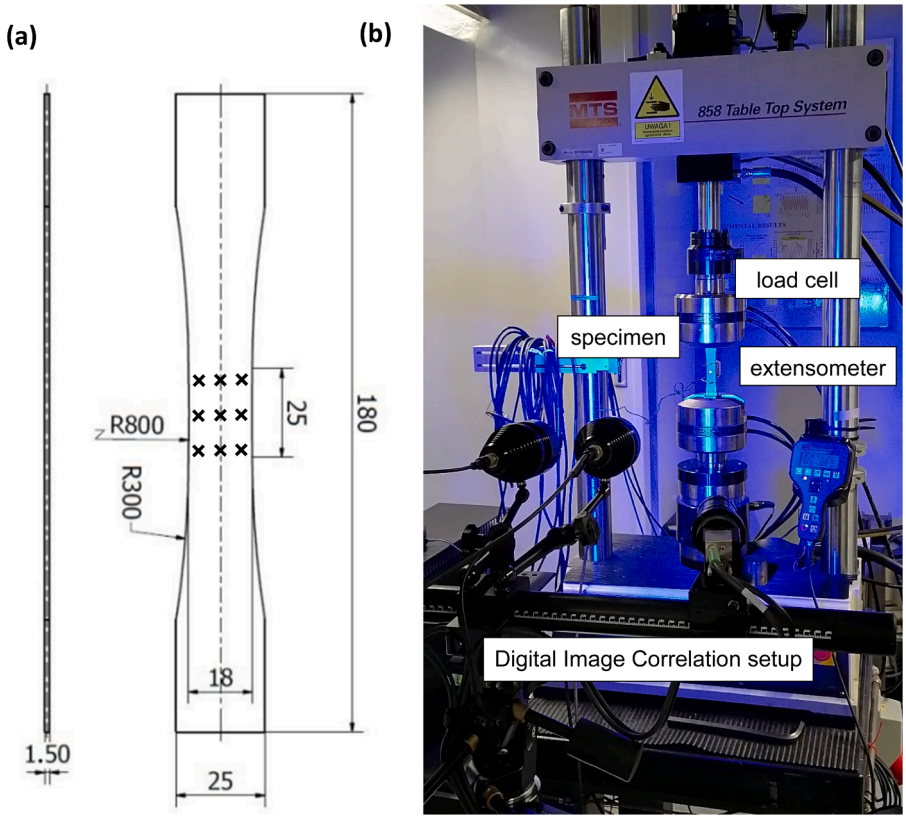

Fig. 1. The engineering drawing of the fatigue specimen (a); testing setup consisting of MTS 858 machine and DIC equipment (b).

measurement range, challenges with attachment, potential failure in harsh environments, and the requirement for multiple strain gauges for various directions [12]. Regardless of many advantages as compared to traditional techniques, one should mention relatively simple experimental setup and quick specimen preparation, measurement efficiency including high precision and stability in wide measurement range and over the entire analysed area, that enable non-contact full field and multipoint measurement even in outdoor environments. On the other hand, the limitations of the DIC method involve the dependence of the measuring accuracy on the natural light conditions and the necessity of artificial light application during high-frequency measurements. Additionally, calibration plates appropriate to the specimen area are required to minimise errors related to the measurement precision and the occurrence of noise due to specific lens quality. Furthermore, notable storage space and hardware are required for data processing. Considering all the advantages and limitations of the DIC method, it is still the most effective technique to monitor potential crack initiation and its development due to fatigue.

Thus, in this paper, DIC-assisted fatigue tests were executed to monitor the strain evolution of 13HMF power engineering steel subjected to LCF in a plastic regime. The data collected from optical measurements were subsequently compared to those registered by the extensometer to assess the effectiveness of the proposed approach. Finally, strain distribution cloud data was generated from DIC measurements with potential application in finite element simulations.

2. Materials and methods

The 13HMF power engineering steel was supplied in the form of a pipe in the as-received state. The chemical composition of the material was presented in Table 1. Specimens were extracted from the pipe section and machined to the geometry presented in Fig. 1a. Such geometry enforces strain accumulation in the central section of the specimen.

Mechanical testing was carried out using a conventional MTS 858 testing machine (Fig. 1b). The experimental programme begins with standard tensile tests at a strain rate of 0.002 s^{-1} to determine yield point and ultimate tensile strength. Fatigue loading conditions were established based on the yield strength value obtained. The tests were performed under force control with a (σ_{max}- σ_{min})/2 level, a stress asymmetry coefficient R = 0, at a frequency of 20 Hz within the stress range ($\Delta\sigma$) of 380 MPa to 500 MPa. Prior to and during fatigue tests, the specimens were pre-stretched to a stress value of +10MPa to prevent buckling. The strain evolution was monitored using a conventional MTS extensometer with a gauge length of 25 mm and DIC Aramis 12M setup. The experimental code was set to automatically capture DIC images every 1000 fatigue cycles at the maximum value of stress amplitude applied. The area of interest for DIC strain measurements was located between the extensometer arms. Nine reference points were used for strain measurements by using DIC as indicated in Fig. 1a. Once the strain accumulation preceding specimen fracture was observed during in-situ DIC strain measurements, the test was interrupted to confirm the

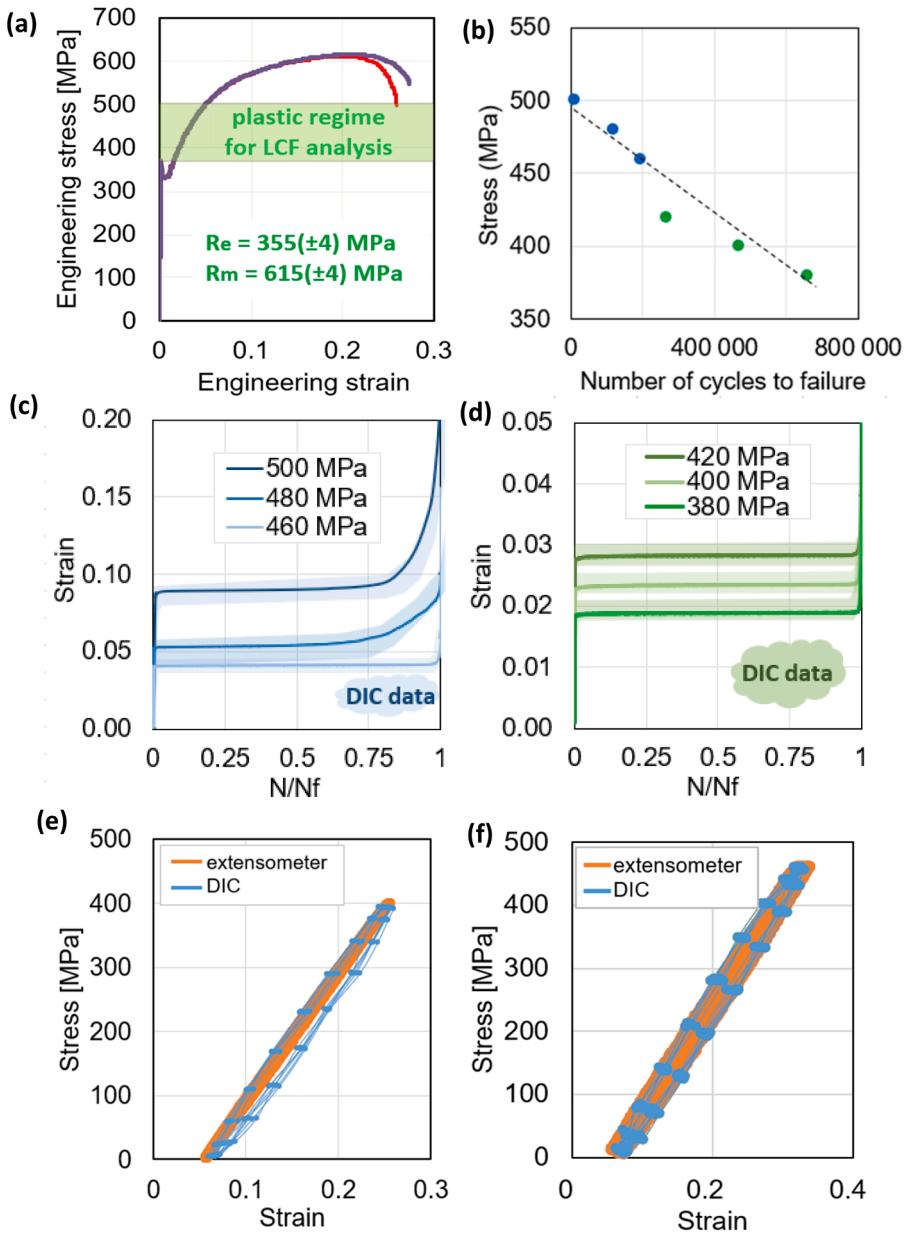

Fig. 2. Stress-strain characteristics of 13HMF power engineering steel with determined LCF region of interest (a); S–N curve (b); comparison of strain evolution registered by extensometer (line) and DIC (shaded area) for different stress amplitudes (c-d); comparison of hysteresis loops in steady-state registered by using extensometer and DIC for material subjected to stress amplitude equal to 400 MPa (e) and 460 MPa (f).

presence of crack by using scanning electron microscopy. The microstructural and fracture surface observations were performed using a JEOL6360LA scanning electron microscope (SEM) operated at 20 kV.

3. Results and discussion

During uniaxial tensile tests, the yield and ultimate tensile strength were determined to be equal to 355 MPa and 615 MPa, respectively (Fig. 2a). Based on the yield strength value, the range of stress amplitude reflecting LCF region was selected. Subsequent fatigue tests were performed to elaborate the S–N curve representing material performance in its plastic regime (Fig. 2b). The strain response was analysed for extremely high (460 MPa, 480 MPa and 500 MPa) and high-stress amplitudes (380 MPa, 400 MPa and 420 MPa) independently, as shown in Fig. 2c and d. One should highlight, that the strain recordings from the extensometer were within those of DIC, but not always in the middle. It could be related to the instability of the extensometer when cyclic loading is applied under a relatively high frequency of 20Hz [13] as well as differences in strain recordings performed by DIC for reference points located near extensometer arms [14]. However, strain evolution captured by both measuring techniques is similar thus extensometer and DIC could be simultaneously and effectively used for mutual validation (Fig. 2e and f).

Once the DIC measurements accuracy was validated through extensometer recordings (Fig. 2e and f), the full-field strain distribution maps were captured for specific values of stress amplitude during specimen loading and unloading (Fig. 3). The representative results for each deformation stage were presented for the stress amplitude equal to 400

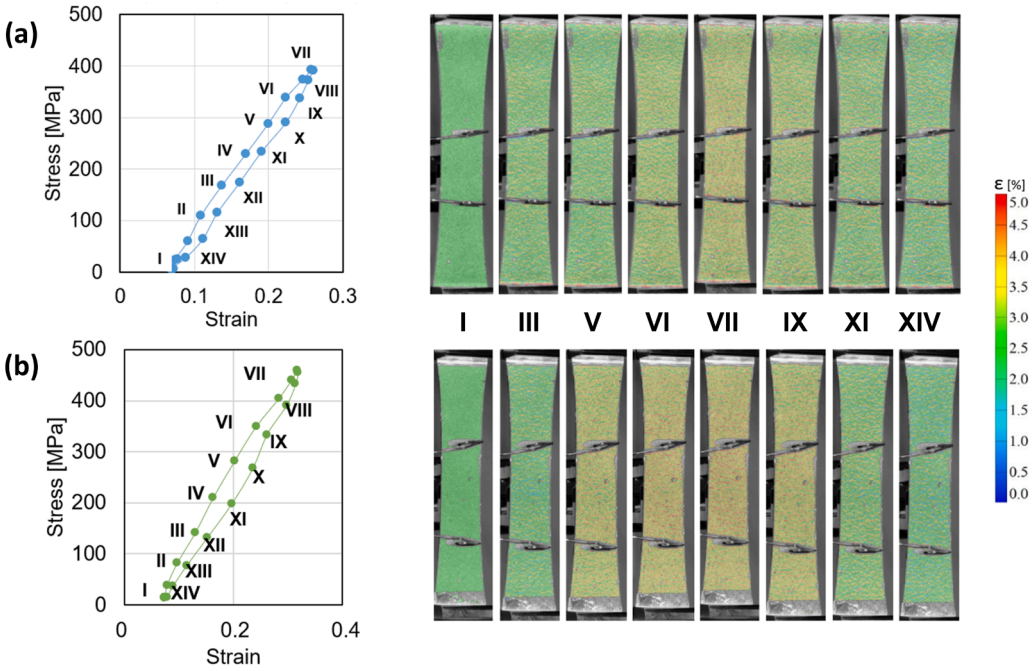

Fig. 3. Determination of hysteresis loop based on the DIC measurements for 13HMF steel subjected to stress amplitude equal to 400 MPa (a) and 460 MPa (b).

MPa (Fig. 3a) and 460 MPa (Fig. 3b). Once the maximum value of stress amplitude was reached in stage VII, the corresponded strain localisation in middle section of strain gauge was found. Since no specific area of strain accumulation was found for initial hysteresis loops, such a DIC approach was continued till specimen fracture.

Strain distribution maps for each fatigue life stage were further elaborated to identify the potential area of crack nucleation (Fig. 4). One can indicate, that for lower values of stress amplitude equal to 380 MPa and 400 MPa, the strain concentration could be observed already in the middle stage of service life as indicated by yellow arrows for 0.5 N/Nf. The stable crack growth was steadily progressing till specimen fracture. It should be highlighted, that for both these amplitudes, the strain recordings do not exceed 5 % and the area of the highest strain accumulation could be found near the crack initiation. Therefore, it was concluded that DIC could be effectively used to precisely indicate the potential area of failure already in the early stage of fatigue damage development. On the other hand, the testing at higher stress amplitudes equal to 460 MPa, 480 MPa and 500 MPa led to significant strain accumulation in almost the entire gauge area located between extensometer arms. Such deformation was directly related to the significant plastic deformation introduced to the specimen already at the beginning of the test [15,16]. The specimen subjected to cyclic loading at a stress amplitude equal to 480 MPa was characterised by notable strain accumulation in its central part represented by intersecting bands of high strain values. This behaviour could be related to the initiation of cracks in more than one area due to specimen imperfection or inclusions located near the edge [17]. Different behaviour was found during testing at a stress amplitude of 500 MPa, where the strain was evenly distributed in the gauge section.

Although both the extensometer and DIC ARAMIS optical systems measure strain with the ISO 9513's 0.5 class of accuracy, strain recordings registered in a steady state of material subjected to specific values of stress amplitude expose significant differences (Table 2). They might be attributed to the rapid crack growth during last stage of fatigue. Once the crack initiates and propagates, local strain values registered by DIC in the crack area are extremely high. On the other hand, the stable recordings from the extensometer provide the average value of strain changes recorded in the 25 mm long gauge. Even though the crack appears, it is hard to confirm its presence having data from the extensometer. Therefore, it was confirmed, that the DIC methodology is more effective in the early detection of crack initiation and further propagation monitoring.

The character of hysteresis loops observed for 13HMF steel (Fig. 2e and f) suggested the occurrence of the ratcheting effect, which is defined as an accumulation of plastic strain under cyclic loading [18]. Such material behaviour was more prominent when higher stress amplitude was applied as could be observed in Fig. 2f. A similar finding was also reported by Paul et al. [18] who investigated the LCF performance of SA333 steel for which, ratcheting strain rate increases with an increase in mean stress or stress amplitude. Although ratcheting may be considered the main deformation mechanism, one should note the difference between LCF behaviour and the ratcheting phenomenon. It was reported, that ratcheting fatigue lives are significantly lower than the LCF ones and it is due to the accumulation of tensile ratcheting strain over cycles [19]. Furthermore, ratcheting results in permanent strain accumulation with cycling therefore the ratcheting strain accumulation increases with increasing mean stress for constant stress amplitude. Such findings highlight the importance of load control testing since for progressive cycles, engineering stress-controlled experiments exhibited an abrupt increase in strain and hence reduced service life could be found for the same material subjected to the true stress-controlled tests [20]. It is an extremely important issue in the fatigue testing and damage monitoring in piping materials, such as 13HMF or SA333 steel [18,20]. Since these materials operate under significant internal pressure, they may experience ratcheting due to cyclic loading from plant start-up, shut-down and changing operating conditions [20]. Ratcheting can lead to permanent deformation in piping components, such as ovalisation of T-joints and elbows during cyclic bending, thinning of cross-sectional areas, and local bulging of pressurised pipes under cyclic loading [20]. Therefore, it is crucial to analyse the material's behaviour under different loading conditions to ensure the efficient design of piping systems. It is also of the highest importance to understand

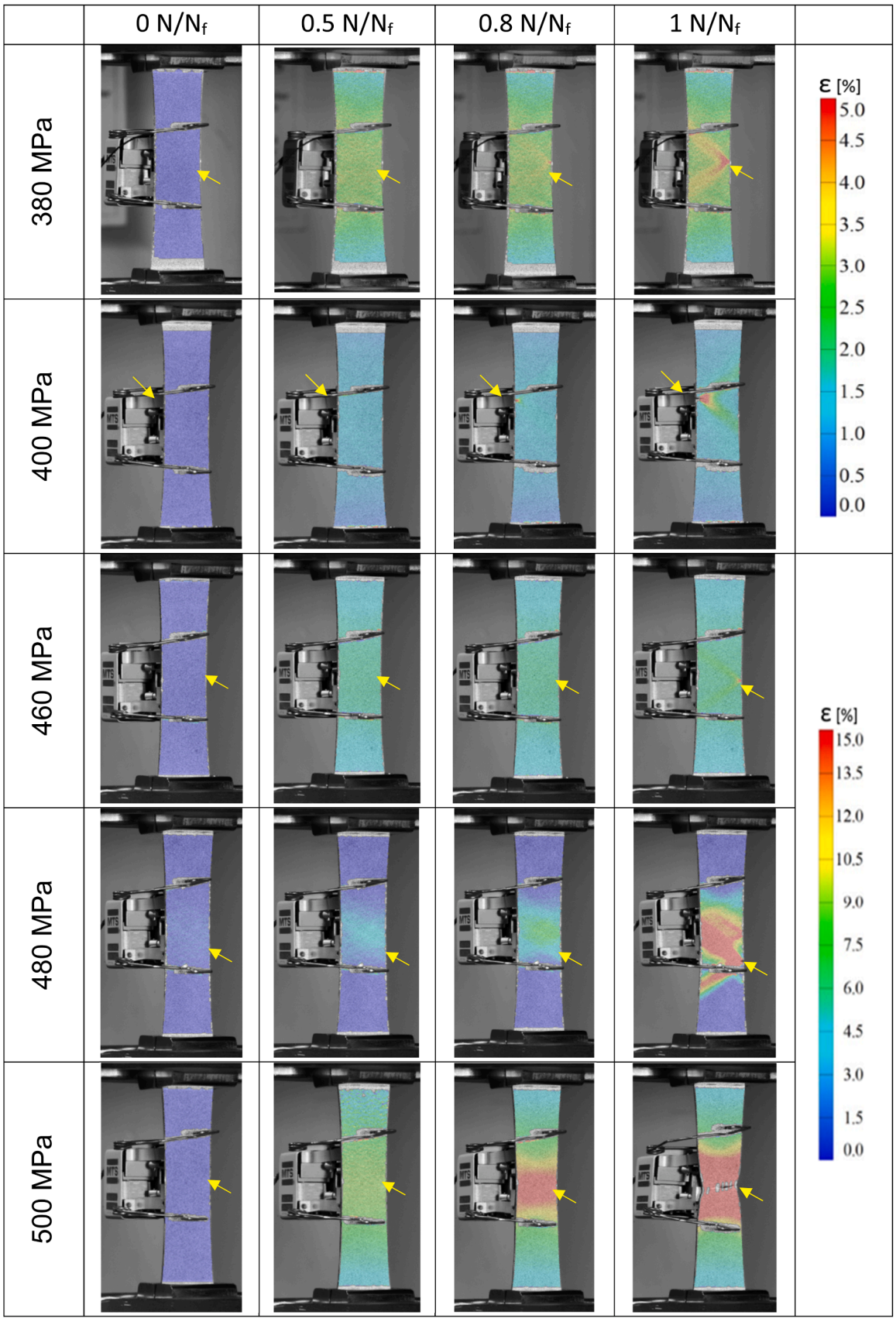

Fig. 4. DIC strain evolution maps for 13HMF power engineering steel subjected to LCF

Table 2
Strain recordings for steady-state of 13HMF subjected to cyclic loading as measured by extensometer and DIC

	500 MPa	480 MPa	460 MPa	420 MPa	400 MPa	380 MPa
Extensometer	0.090 ±0.004	0.053 ±0.003	0.041 ±0.003	0.028 ±0.001	0.023 ±0.001	0.018 ±0.001
DIC	0.080 ±0.015	0.051 ±0.010	0.040 ±0.008	0.030 ±0.005	0.022 ±0.005	0.018 ±0.002

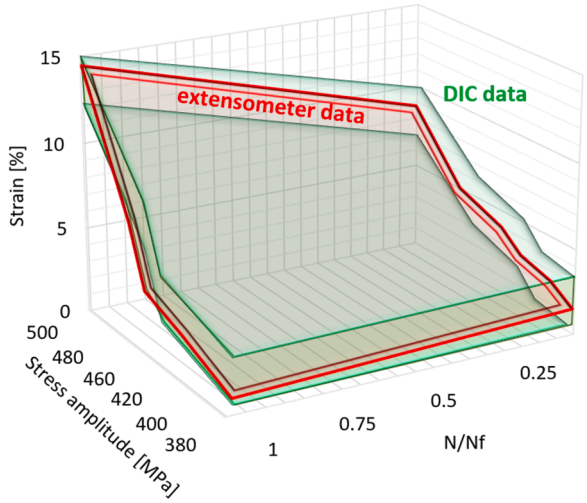

Fig. 5. Strain distribution cloud data generated from DIC measurements executed during fatigue tests for 13HMF power engineering steel tested under different stress amplitudes.

material behaviour under cyclic plastic deformation which involves several aspects: ratcheting, stress-dependent hardening, cyclic hardening/softening, the Bauschinger effect, strain range effect, loading history memory, mean stress relaxation and non-proportional hardening [21]. It was reported, that cyclic hardening/softening depends upon loading types (i.e. stress/strain controlled), loading history and strain/stress range applied during the test. On the other hand, permanent strain accumulation due to ratcheting leads to specimens' cross-sectional area reduction which in turn causes unpredictable changes in true stress during engineering stress-controlled ratcheting experiments [21].

The multi-level point cloud post-processing for the point cloud optimisation of multi-view images in the DIC system plays a crucial role in enhancing the accuracy of DIC measurement [22]. Therefore, in this research, a new approach was proposed to address such issues. Data from DIC measurements generated during fatigue tests was used to visualise the strain distribution of 13HMF power engineering steel subjected to cyclic loading under different stress amplitudes (Fig. 5). One could observe a stable strain increase registered for stress amplitudes ranging from 380 MPa to 420 MPa. On the other hand, the adoption of its higher values is leading to a significant strain increase already at the beginning of the test. The further exposure to cyclic loading leads to drastic material softening reflected by a non-stable strain increase, which is causing specimen fracture. One should highlight, that the surfaces generated from DIC measurements represent maximum and minimum strain evolution strain planes in the form of a cloud of points for the entire test, till specimen fracture. Therefore, the area between them is suitable for finite element calculations as it corresponds to the real-time material behaviour operating under cyclic loading. It could be observed, that the results recorded from extensometer recordings were located between these DIC-generated strain planes. Although such results should represent average values recorded for the specific strain gauge, it was noticed that strain varies significantly.

Due to the local nature of fatigue damage initiation and following development, the DIC data from strain measurements were also analysed along the loading direction applied and subsequently correlated with SEM observations executed in the area of potential crack initiation (Fig. 6). It was observed, that for the relatively low value of stress amplitude equal to 380 MPa, crack initiation was found after exceeding a midlife state of the specimen (~0.75 N/Nf) (Fig. 6a). It was followed by its stable growth till specimen fracture. However, the strain distribution measured on the entire area of the specimen was at a similar, constant level. The microstructural observations performed in the area of strain accumulation confirmed the occurrence of cracks. Although the length of the crack was notably lower than the accuracy of the DIC setup, its presence was detected in the area where strain values increased (Fig. 6a–c). Such behaviour was also observed for the specimens subjected to stress amplitudes equal to 400 MPa (Fig. 6b) and 460 MPa (Fig. 6c). Therefore, it was confirmed, that once the crack nucleates, it cannot be precisely detected by extensometer recordings since it provides average values from the gauge length. On the other hand, the strain distribution registered for the specimens subjected to the stress amplitudes equal to 480 MPa and 500 MPa presents different behaviour (Fig. 6d and e). The strain accumulation was already found in the initial cycles due to significant plastic deformation introduced in the first loading cycles. As could be observed in Fig. 6d, there were two initiation sites found on the specimen surface when testing was performed at 480 MPa: one in the middle section of gauge length, and a second near its bottom part. Although the strain accumulation was more pronounced in the central part, the decohesion occurred at the bottom. Such behaviour was also notable during microstructural observations. The area of strain accumulation subjected to SEM analysis revealed multiple cracks formed in the area significantly narrower than the one exposed by DIC measurements.

Based on strain distribution on the specimen surface registered by DIC at each stress amplitude (Figs. 4 and 6), one can confirm the local nature of crack initiation during fatigue. While the extensometer strain recordings are represented by one set of average data obtained from the gauge, DIC maps and strain evolution profiles could effectively identify the deformation changes on the entire specimen surface. For the most investigated cases, the crack nucleate in one specific area early indicated by the DIC as a potential region characterised by significant strain fluctuations. One should highlight that the coupled approach of strain profiles and maps provides significantly more information than traditional DIC qualitative measurement. Since the same colour is used to illustrate similar strain values, it is hard to identify the potential area of failure as could be observed for the specimen subjected to a stress amplitude of 480 MPa (Fig. 4). However, the strain profiles could clearly indicate such area as shown in Fig. 6d. One should highlight, that high-resolution DIC offers similar strain measurement possibilities as the approach presented, however, most of those studies concern notched specimens during fatigue [22-25] or simple, uniaxial deformation [26] only. Therefore, the presented approach may serve as a bridge between macro-micro measurements, that further enable understanding of the material behaviour when a notch is not applied [27].

The observations of fracture surfaces after specimen failure revealed no significant changes in fracture mode between specimens subjected to different values of stress amplitude (Fig. 7). Since the fatigue testing was performed in the LCF regime, all specimens exhibited ductile fracture represented by dimples of various sizes, voids and craters with inclusions found inside them. The higher the stress amplitude was, the larger dimples and craters were found. Such material behaviour was

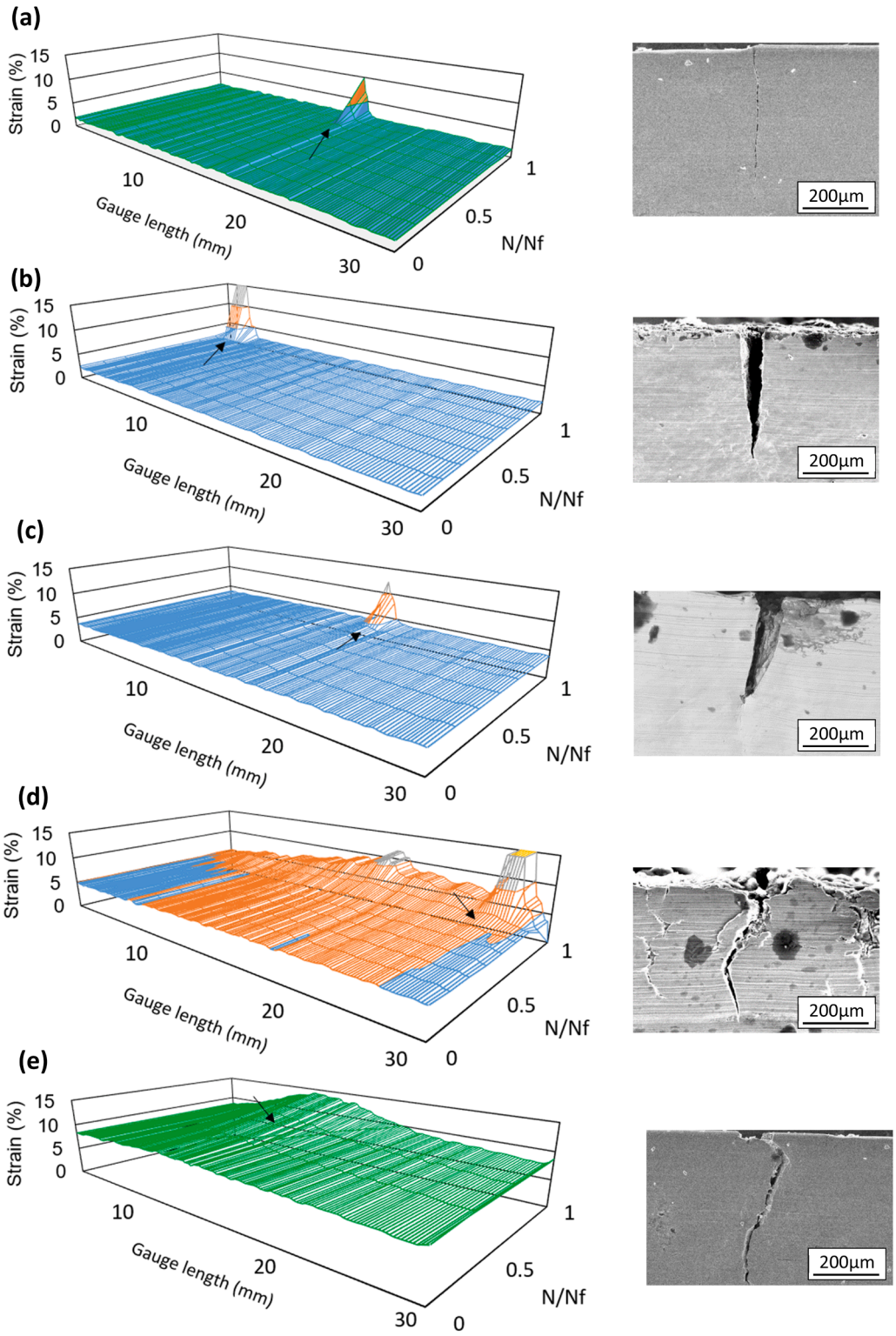

Fig. 6. Strain evolution profiles derived from DIC measurements executed during fatigue tests of 13HMF power engineering steel tested under stress amplitude equal to 380 MPa (a), 400 MPa (b), 460 MPa (c), 480 MPa (d) and 500 MPa (e).

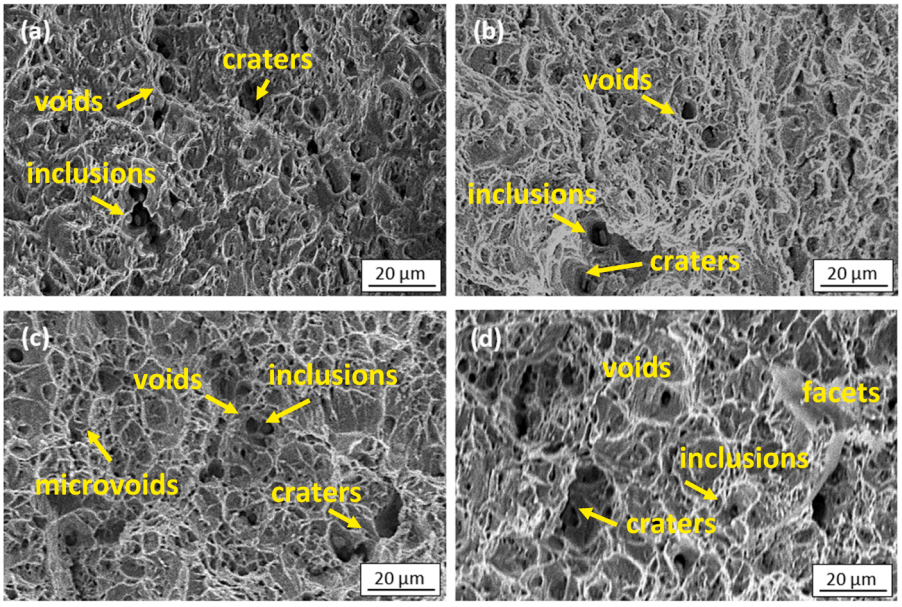

Fig. 7. Fracture surfaces of 13HMF power engineering steel after fatigue under stress amplitude equal to 380 MPa (a), 400 MPa (b), 480 MPa (c) and 500 MPa (d).

directly related to the interaction between ductile matrix and inclusions of significantly higher hardness. These inclusions act as stress concentrators and accelerate fatigue damage development in the LCF regime.

In order to further explore the fracture mechanisms of 13HMF steel subjected to fatigue, microscopic observations were performed in specific areas of each specimen (Fig. 8). The examination of the fatigue crack source area in all specimens revealed a ductile fracture mode characterised by fine dimples evenly distributed on the surface. However, the ductile nature of the fracture was slightly different and depended on the stress amplitude applied. The specimens tested at a stress amplitude equal to 380 MPa and 400 MPa were characterised by a coarse surface with a notable number of craters containing inclusions and microvoids. The distinct shape of these craters and surrounding cleavage facets may be attributed to the crack initiation due to stress accumulation on the inclusion-matrix boundary. Consequently, plastic strain propagation was initiated near these inclusions acting as stress concentrators [28]. Conversely, the presence of smaller microvoids near inclusions is due to the interaction between hard, brittle inclusions and the metal matrix. In contrast, specimens tested at stress amplitude equal to 480 MPa and 500 MPa displayed fracture surfaces predominantly covered with fine dimples. The inclusions within the craters were of similar size, indicating fatigue interaction with the matrix. The DIC measurements (Figs. 4 and 6) correlated with microscopic observations (8) exposed various damage mechanisms associated with the stress amplitude adopted. When the stress amplitude equal to or lower than 460 MPa was applied, the crack initiation was found on the specimen edge in the form of a single, thin crack (Fig. 6a–c). It steadily propagates through the entire width of the specimen resulting in the formation of secondary cracks (Fig. 8). On the other hand, the specimens tested under a stress amplitude of 480 MPa and 500 MPa displayed a strain accumulation area in the central region of the gauge (Fig. 6d and e). In the middle section, a strong interaction between inclusions and the matrix was observed, with a large area of fine dimples found below non-metallic particles (Fig. 8). The crack propagated towards the edges of the specimen, where the material remained coherent. Excessive stress in the external areas resulted in the formation of microvoids in the plastically deformed edges. Despite different fracture mechanisms, all specimens exhibited classical phenomena of cyclic plastic deformation, microcrack initiation, coalescence, and macroscopic crack formation.

4. Conclusions

In this paper, the quantitative DIC approach was effectively used to monitor fatigue damage development of 13HMF power engineering steel subjected to LCF. The data generated from DIC measurements were validated through extensometer recordings to further confirm the suitability of full-field optical methodology for fatigue monitoring. Furthermore, it was possible to predict the potential area of crack initiation after exceeding the midlife of a specimen subjected to cyclic loading by using strain distribution maps generated during automatic surface monitoring as confirmed by SEM observations. Additionally, the surface derived from DIC measurements represented the strain development in the form of a cloud of points throughout the entire test, until specimen fracture. Hence, the area below is well-suited for finite element calculations as it reflects the real-time material behaviour under cyclic loading.

Funding

This work has been partially supported by the National Science Centre through grant no. 2019/35/B/ST8/03151.

CRediT authorship contribution statement

Mateusz Kopec: Writing – review & editing, Writing – original draft, Visualization, Validation, Supervision, Software, Resources, Project administration, Methodology, Investigation, Formal analysis, Data curation, Conceptualization.

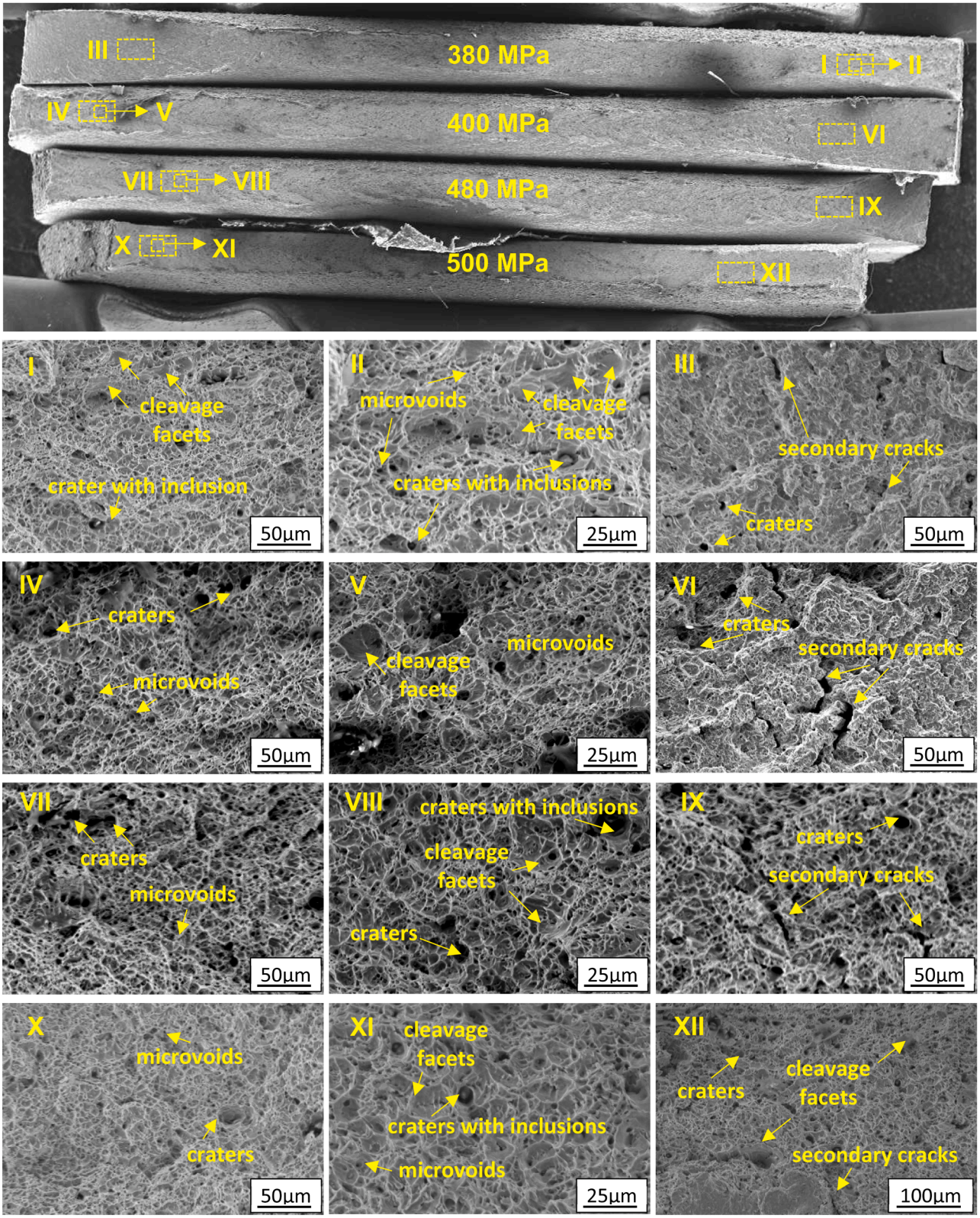

Fig. 8. Detailed fracture surface analysis of 13HMF power engineering steel after fatigue tests executed in the specific areas of the specimen

Declaration of competing interest

The authors declare that they have no known competing financial interests or personal relationships that could have appeared to influence the work reported in this paper.

Data availability

Data will be made available on request.

Acknowledgements

The author would like to express his gratitude to Prof. Z.L. Kowalewski for fruitful discussions, Mr Adam Brodecki and Mr M.Wyszkowski for their kind help during the experimental part of this work.

References

[1] Kopec M, Kukla D, Brodecki A, Kowalewski ZL. Effect of high temperature exposure on the fatigue damage development of X10CrMoVNb9-1 steel for power plant pipes. Int J Pres Ves Pip 2021;189:104282. https://doi.org/10.1016/j.ijpvp.2020.104282.
[2] Arumugam T, Vijaya Kumar SD, Karuppanan S, Ovinis M. The influence of axial compressive stress and internal pressure on a pipeline network: a review. Appl Sci 2023;13(6):3799. https://doi.org/10.3390/app13063799.
[3] Gwoździk M, Motylenko M, Rafaja D. Microstructure changes responsible for the degradation of the 10CrMo9-10 and 13CrMo4-5 steels during long-term operation. Mater Res Express 2020;7:016515. https://doi.org/10.1088/2053-1591/ab5fc8.
[4] Golański G, Kolan C, Jasak J. Degradation of the microstructure and mechanical properties of high-chromium steels used in the power industry. In: Tanski T, Sroka M, Zielinski A, editors. Creep. London: IntechOpen. editors 2017. https://doi.org/10.5772/intechopen.70552.
[5] Singh K, Kamaraj M. Microstructural degradation in power plant steels and life assessment of power plant components. Procedia Eng 2013;55:394–401. https://doi.org/10.1016/j.proeng.2013.03.270.
[6] Piotrowski L, Chmielewski M, Golański G, Wieczorek P. Analysis of the possibility of creep damage detection in T24 heat resistant steel with the help of magnetic nondestestructive testing methods. Eng Fail Anal 2019;102:384–94. https://doi.org/10.1016/j.engfailanal.2019.04.054.
[7] Curt J, Capaldo M, Hild F, Roux S. An algorithm for structural health monitoring by digital image correlation: proof of concept and case study. Opt Lasers Eng 2022;151:106842. https://doi.org/10.1016/j.optlaseng.2021.106842.
[8] Chu TC, Ranson WF, Sutton MA. W.H. Peters Application of digital-image-correlation techniques to experimental mechanics. Exp Mech 1985;25:232–44. https://doi.org/10.1007/BF02325092.
[9] Hebert J, Khonsari M. The application of digital image correlation (DIC) in fatigue experimentation: a review. Fatigue Fract Eng Mater Struct 2023;46(4):1256–99. https://doi.org/10.1111/ffe.13931.
[10] J. Forster, A. Theobald, S. Engel, R. Pasmann Using optical measuring system for identification of material parameters for finite element analysis. In: 11. LS-DYNA, DYNAmore GmbH, Ulm, (2012) pp 1–9.
[11] Durif E, Réthoré J, Combescure A, Fregonese M. Chaudet Controllingstress intensity factors during a fatigue crack propagation using digital imagecorrelation and a load shedding procedure. Exp Mech 2012;52:1021–31. https://doi.org/10.1007/s11340-011-9552-6.
[12] Kopec M, Brodecki A, Kukla D, et al. Suitability of DIC and ESPI optical methods for monitoring fatigue damage development in X10CrMoVNb9-1 power engineering steel. ArchivCivMechEng 2021;21:167. https://doi.org/10.1007/s43452-021-00316-1.
[13] McEnteggart I. Extensometers. In: Sharpe W, editor. Springer Handbook of Experimental Solid Mechanics. Boston, MA: Springer Handbooks. Springer; 2008. https://doi.org/10.1007/978-0-387-30877-7_13.
[14] Bornert M, Brémand F, Doumalin P. Assessment of Digital Image Correlation Measurement Errors: Methodology and Results. Exp Mech 2009;49:353–70. https://doi.org/10.1007/s11340-008-9204-7.
[15] Ren W, Nicholas T. Effects and mechanisms of low cycle fatigue and plastic deformation on subsequent high cycle fatigue limit in nickel-base superalloy Udimet 720. Mater Sci Eng A 2002;332(1–2):236–48. https://doi.org/10.1016/S0921-5093(01)01742-7.
[16] Paul SK. A critical review of experimental aspects in ratcheting fatigue: microstructure to specimen to component. JMR&T 2019;8(5):4894–914. https://doi.org/10.1016/j.jmrt.2019.06.014.
[17] Serrano-Munoz I, Buffiere JY, Mokso R, Verdu C, Nadot Y. Location, location & size: defects close to surfaces dominate fatigue crack initiation. Sci Rep 2017;27(7):45239. https://doi.org/10.1038/srep45239.
[18] Paul SK, Sivaprasad S, Dhar S, Tarafder S. Ratcheting and low cycle fatigue behavior of SA333 steel and their life prediction. J Nucl Mater 2010;401(1–3):17–24. https://doi.org/10.1016/j.jnucmat.2010.03.014.
[19] Paul SK, Stanford N, Taylor A, Hilditch T. The effect of low cycle fatigue, ratcheting and mean stress relaxation on stress–strain response and microstructural development in a dual phase steel. Int J Fatigue 2015;80:341–8. https://doi.org/10.1016/j.ijfatigue.2015.06.003.
[20] Paul SK, Sivaprasad S, Dhar S, Tarafder S. True stress control asymmetric cyclic plastic behavior in SA333 C–Mn steel. Int J Pres Ves Pip 2010;87:440–6. https://doi.org/10.1016/j.ijpvp.2010.07.008.
[21] Paul SK, Sivaprasad S, Dhar S, Tarafder S. Key issues in cyclic plastic deformation: experimentation. Mech Mater 2011;43:705–20. https://doi.org/10.1016/j.mechmat.2011.07.011.
[22] Ge P, Wang Y, Zhou J, Wang B. Point cloud optimization of multi-view images in digital image correlation system. Opt Laser Eng 2024;173:107931. https://doi.org/10.1016/j.optlaseng.2023.107931.
[23] Carroll JD, Abuzaid W, Lambros J, Sehitoglu H. High resolution digital image correlation measurements of strain accumulation in fatigue crack growth. Int J Fatigue 2013;57:140–50. https://doi.org/10.1016/j.ijfatigue.2012.06.010.
[24] Vanlanduit S, Vanherzeele J, Longo R, Guillaume P. A digital image correlation method for fatigue test experiments. Opt Laser Eng 2009;47(3–4):371–8. https://doi.org/10.1016/j.optlaseng.2008.03.016.
[25] Lipiäinen K, Afkhami S, Ahola A, Björk T. Evaluation of geometrical notch and quality effects in the fatigue strength assessment of ultra-high-strength steel cut edges. Structures 2022;37:881–92. https://doi.org/10.1016/j.istruc.2022.01.069.
[26] Jedidi MY, Valle V. Experimental investigation to determine necking of commercially pure titanium sheets using a time-of-flight camera and Heaviside-digital image correlation. Opt Laser Eng 2023;164:107529. https://doi.org/10.1016/j.optlaseng.2023.107529.
[27] Liu M, Li X. Mechanical properties measurement of materials and devices at micro- and nano-scale by optical methods: a review. Opt Laser Eng 2022;150:106853. https://doi.org/10.1016/j.optlaseng.2021.106853.
[28] Lin S, Wang D, Li C, Liu X, Di X, Jiang Y. Effect of cyclic plastic deformation on microstructure and mechanical properties of weld metals used for reel-lay pipeline steels. Mater Sci Eng A 2018;737:77–84. https://doi.org/10.1016/j.msea.2018.09.036.